

Thickness Dependent Effects of Thermal Annealing and Solvent Vapor Treatment of Poly (3-hexylthiophene) and Fullerene Bulk Heterojunction Photovoltaics

Zhouying Zhao¹, Lynn Rice¹, Harry Efstathiadis¹ and Pradeep Haldar^{1*}

¹College of Nanoscale Science and Engineering, University at Albany, State University of New York, 255 Fuller Road, Albany, NY 12203, U.S.A.

ABSTRACT

We have utilized room-temperature solvent vapor treatment followed by thermal annealing to process bulk heterojunction (BHJ) photovoltaic devices based on blends of poly (3-hexylthiophene) (P3HT) and phenyl-C61-butyric acid methyl ester (PCBM) of varied active layer thickness. The morphological and photovoltaic performance characteristics of the cells subject to these treatments were found to be dependent on active layer thickness. The devices were characterized using atomic force microscopy (AFM) and opto-electrical and external quantum efficiency measurements in order to analyze the mechanism underlying the observed trend. Performance indicators including fill factor, short-circuit current and power conversion efficiency were correlated to the ordering of device active layers and morphology. The maximum power conversion efficiency achieved was 4.1 %.

INTRODUCTION

From the earliest work [1] onward, and particularly with the advent of bulk heterojunction (BHJ) as opposed to bilayer processing [2], the P3HT/PCBM system has emerged as a model system for organic photovoltaic devices because of the system's balanced charge transfer and high absorption in the visible range. In comparison to silicon-based photovoltaics, organic PV devices are easier to process and potentially more economical [3]. To date, record power conversion efficiency of over 6 percent has been achieved by optimizing processing in the P3HT/PCBM system [4].

The effect of active layer annealing in BHJ photovoltaic devices based on blends of these materials is of special interest because the ultimate cell performance and efficiency bear a strong dependence on the annealing method and conditions.

Optimizations that take annealing into consideration have been performed a number of times on the P3HT/PCBM heterojunction system, resulting in state-of-the-art power conversion efficiencies. [5-8]. Features seen upon thermal annealing of these BHJ devices include increased photon absorption, reduced series resistance of the bulk blend film, and better contacts with the cathode and anode [5].

The addition of PCBM to P3HT disrupts P3HT ordering and annealing facilitates phase separation and restores the polymer to its pristine state of ordered structure [9, 10]. Annealing increases the P3HT molecule chains' π - π overlap, resulting in a red shift of the absorption maxima [11]. Higher crystallinity of P3HT and more fluidic mobility of fullerenes in the BHJ

mesophase resulting in the fullerenes' uniform dispersion within the layer dramatically effects PV performance [12]. With ordering and formation of PCBM aggregates comes marked differences in charge carrier mobility and solar energy absorption which improves the short circuit current (I_{sc}), fill factor (FF) and open circuit voltage (V_{oc}) in annealed devices [3, 10, 13]. Explicitly, a modification in hopping mechanisms seen in annealed BHJ systems results in lower hopping activation energies because of improved charge carrier mobility in the active layer [14].

With respect to processing, Y. Kim et al noted that the solvent plays a role in modifying film morphology, finding that active layers cast from chlorobenzene demonstrated more ordered mesophase morphology and ultimately performed more efficiently than those cast from dichlorobenzene [15].

Their work concluded that the observed preferential solvent effects were rooted in the different evaporation speed of the active layer during processing. Their conclusion was corroborated by experiments in which the only variable was evaporation speed [16]. In fact, it was also observed that, for certain evaporation speeds, no thermal anneal was necessary to restore P3HT crystallinity.

Photocurrent and mobility measurements performed on slowly and quickly evaporated layers indicate that hole mobility is reduced and hole transport is more dispersive in quickly evaporated layers (though there is a higher electron mobility), while, in slowly evaporated layers, hole transport is more non-dispersive and enhanced [17].

The ability to create nanocrystalline P3HT/PCBM domains absent heat treatment followed the advent of the recent solvent vapor treatment, in which the BHJ cells are subjected to solvent vapors at room temperature. Solvent vapor treatment has been observed to have a similar effect as thermal annealing, with solvent vapor-treated samples ultimately achieving higher power conversion efficiencies than their thermally-annealed counterparts, in part due to the fact that they are not subject to thermal stress [19, 20].

Even more recently, researchers found that devices subjected to a combination of solvent vapor treatment and thermal annealing perform better than otherwise identically processed devices subjected to either process alone. They propose that solvent vapor treatment activates self-organization of the P3HT molecule chains, while thermal annealing activates diffusion and aggregation of PCBM [21]. Still, an understanding of the precise mechanism behind annealing and corresponding interpenetrating of P3HT/PCBM BHJ, and recorded relationships governing annealing process conditions and their direct effect on cell performance, remains to be developed.

We have investigated the effect of solvent treatment and thermal annealing processes and found these effects to be specific to active layer thickness. In this work, we performed solvent and thermal annealing on samples of various thicknesses and found that, not only is there is a systematic change in performance upon device annealing that is contingent on active layer thickness, but that, at some critical thickness, an inflection point is observed where the effect of thermal annealing switches from improving device performance to degrading device performance.

EXPERIMENT

Our photovoltaic devices were fabricated on commercially pre-patterned indium tin oxide coated glass slides. The substrates were pre-cleaned in an ultrasonic bath of deionized water and

then treated in UV-Ozone using Jelight UVO cleaner. Polyethylenedioxythiophene- poly styrene sulfonate (PEDOT-PSS) (Baytron P) was spin-coated onto the substrates and annealed at 170° C for 4 min to form a 60 nm -thick film.

Prior to cell fabrication, a solution consisting of 17 mg/mL regioregular P3HT (from Rieke Metals, Inc.) in 1,2-dichlorobenzene was added to PCBM (from American Dye Source, Inc) in a 1:0.6 weight ratio and then stirred at 45 °C for 36 h in a light-protected environment in nitrogen ambient.

The substrates were transferred inside a nitrogen-filled glove box where an active layer was spin coated from the P3HT/PCBM solution at speeds of 500, 1500 and 2000 rpm for 60 s. Each of the substrates was transferred to a plastic container and exposed to vapor of the residual solvent. A ~1 nm thick layer of cesium fluoride followed by a 40 nm thick top contact of aluminum were thermally evaporated onto the active layer in a vacuum chamber located inside the glove box.

The as-prepared cell performance was measured under AM 1.5 illumination using a halogen lamp solar simulator in a nitrogen environment at room temperature. The lamp had been calibrated to 100 mW/ cm² with a Si photodiode (Edmund optics) coupled to an integrating sphere. Current-voltage measurements were collected with a Keithley 237 source measurements unit. The devices were then annealed at 160 ° C for 8 min and their photovoltaic performance was again tested under the same conditions. External quantum efficiency (EQE) measurements of the annealed cells were performed using an Oriel Instruments 1000 W Xenon lamp with a monochromator and a Newport power meter outside the glove box after the device area was encapsulated with an epoxy-like layer. Film surface morphology was measured by tapping mode AFM using a Digital Instruments Nanoscope. The thickness measurements were conducted on an Alpha step profilometer and confirmed by scanning electron microscopy. The quantum efficiency was obtained from short circuit current and light intensity of monochromic wavelength illumination. Four to six devices were measured for each type or set of samples that have an active area per device of 3 mm².

RESULTS AND DISCUSSION

We have fabricated three sets of photovoltaic devices with active layer thicknesses of 100 nm, 160 nm and 200 nm (with an accuracy of +/- 5 nm), corresponding to spin casting speeds of 1500 rpm, 1000 rpm and 500 rpm, respectively. Each set of devices was then subjected to a degree of specific solvent anneal (solvent vapor treatment) depending on the spin speed used and residual solvent left, followed by an identical thermal anneal. Typical diode characteristic curves were obtained before and after thermal annealing for all devices fabricated. Figure 1 compares

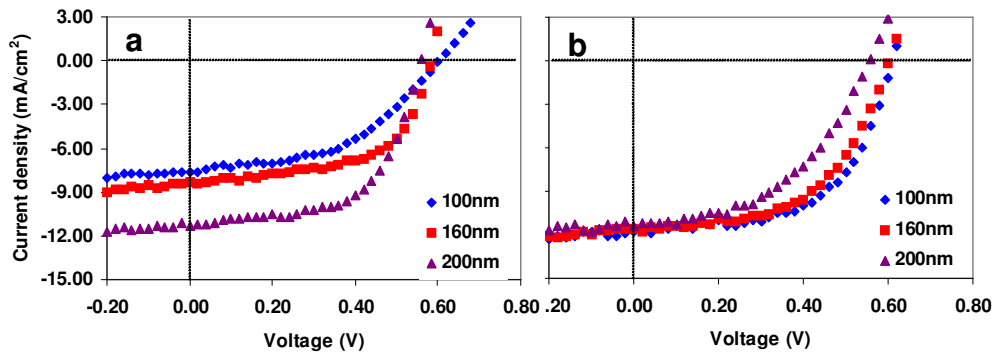


Figure 1. Light I-V curves for P3HT/PCBM heterojunction photovoltaic cells with different active layer thickness as marked in the figure (a) solvent annealing only and (b) solvent/thermal annealing.

the current versus voltage (I-V) characteristics under AM1.5 illumination from the devices receiving solvent vapor treatment only and solvent/thermal annealing, respectively. As seen from the figure, the best photovoltaic performance was initially obtained from the 200 nm device with solvent vapor treatment (Figure 1 (a)) but subsequently obtained from the 100 nm device with followed thermal annealing (Figure 1 (b)). This trend is repeated for the other devices of the same active layer thickness as seen from the power conversion efficiency variations with the annealing treatments depicted in Figure 2.

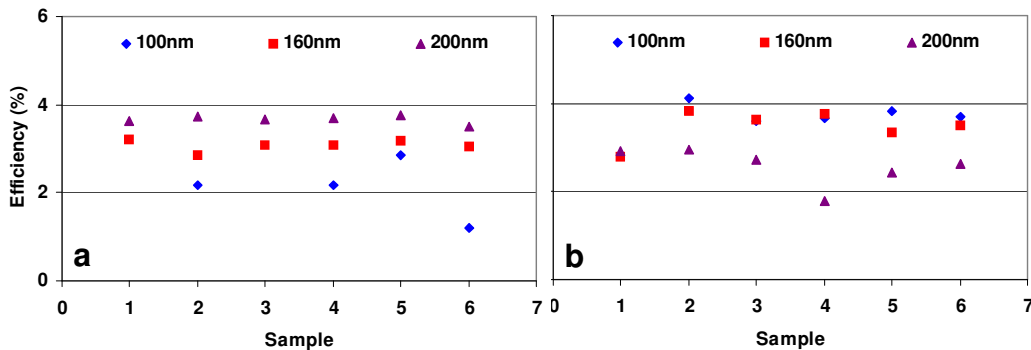


Figure 2. Effect of annealing treatment on power conversion efficiency of P3HT/PCBM heterojunction photovoltaic cells of different active layer thickness: (a) solvent annealing only and (b) solvent/thermal annealing. With solvent annealing, the 200 nm-thick cell exhibits the highest performance, while after solvent/thermal annealing, the 100 nm-thick cell exhibits the best performance.

The statistics of the overall performances were obtained for the devices described above. Before thermal annealing or after solvent vapor treatment, the 100 nm devices had an average power conversion efficiency of 2.1 %, average FF of 0.46 and average V_{oc} of 0.58 V. After thermal annealing, the cell performance parameters improved to average efficiency of 3.7 %, FF of 0.55 and V_{oc} of 0.6 V, while the best performing device exhibited an efficiency of 4.1%.

The solvent vapor treated 160 nm devices showed 3.1 % efficiency and had FF of 0.62 and V_{oc} of 0.57 V. After thermal annealing, the average FF of these devices dropped to 0.52, while the V_{oc} increased to 0.59 and efficiency increased to 3.5 %.

The 200 nm thick devices had 3.5% efficient after solvent annealing, with average FF of 0.58 and V_{oc} of 0.56. Upon thermal annealing, all of these parameters decreased, resulting in 2.5% average efficiency, FF of 0.43 and V_{oc} of 0.55.

Generally, the purpose of annealing PCBM/P3HT BHJ devices is to restore or allow the crystallization of P3HT that is disrupted in the presence of PCBM during device processing [9-14]. While both thermal annealing and solvent vapor treatment techniques improve P3HT ordering, the mechanism by which each technique does so is different, and hence device conditions before thermal annealing have a significant impact on the ultimate effect of the annealing on developed cell performance.

Within the range of active layer thickness investigated, our results indicate that the annealing effect on power conversion efficiency is dependent on film thickness. While thermal annealing was shown to generally improve power conversion efficiency in optimized devices [4], we present a set of devices with relatively thick active layers that don't conform to this broad trend; their performance is systematically lowered upon thermal annealing after solvent vapor treatment.

Here, we make the distinction between "solvent vapor treatment" in which the active layer is not completely dried during the spin coating process and the remainder of the solvent is let to evaporate slowly (what otherwise might be termed "solvent evaporation") and the aforementioned solvent-vapor annealing, in which spin cast, incompletely dried active layers are subject to vapors of solvents such as dichlorobenzene or chlorobenzene to complete phase separation and polymer ordering.

For the thinnest sample (100 nm), the average power conversion efficiency of devices increased from 2.1% to 3.7% in going from the initial solvent treatment step through thermal annealing. For the intermediate thickness sample (160 nm), the average power conversion efficiency of devices did modestly improve from 3.1% up to 3.5% upon thermal annealing. In contrast, for the thickest sample of 200 nm, the average power conversion efficiency after thermal annealing decreased from 3.5% to 2.5%. It is notable that devices identical in every processing aspect except thickness of the active layer had opposite responses to thermal annealing. In thin films less than 160 nm, annealing improved active layer crystallization and networking, while in thick films up to 200 nm, networking was degraded in this thermal anneal step.

The reason for this observed difference in annealing effect stems from the fact that thermal and solvent annealing is mechanistically different. The dominant mechanism of solvent annealing is self assembly of P3HT molecular chains. The thickest films are relatively rich in solvent (and are visibly wet) when undergoing slow spin casting, and hence the P3HT molecules are free to align themselves in this liquid layer and respond dramatically to solvent annealing. The device microstructure domain thereby undergoes significant changes during the solvent annealing of thicker, wetter films [15].

Thinner films have had most of the solvent evaporated in the spin coating step, forcing the P3HT chains into a more rigid phase and little solvent is available to produce an annealing effect on the performance of these devices because most of the solvent had already been evaporated prior to the treatment.

The fragile self organization that is initiated in the solvent annealing step in the thicker films is disrupted by thermal annealing, and the microstructure formed is not maintained. Parts of the networking developed in the solvent evaporation are destroyed by thermal stress [19, 20]. In fact, for thick film devices, this effect of disrupted networking has a stronger influence on device

performance than the positive effect developed in thermal annealing of improving charge transport in the active layer, accounting for a net performance degradation observed upon thermal annealing.

Thinner films, on the other hand, do not receive as much self-organization in the absence of residual solvent and vapor, and hence phase separation and polymer ordering hindered in spin process is not restored effectively. The primary effect observed during thermal annealing is the improved diffusion and aggregation of PCBM clusters and polymer ordering.

The EQE measurements for the thermal annealed cells are plotted in Figure 3. The device with a 100 nm-thick active layer shows a maximum EQE of 67% at 500nm wavelength, a ~18% improvement over the device with a 160 nm-thick active layer. While thicker films still absorb the most light after thermal annealing, as a result of well ordered P3HT [11], the absorbance of light does not correspond to improved efficiency. In fact, the opposite trend is observed: the best performance is achieved in the 100 nm active layer devices. This trend suggests that both microstructure and polymer ordering in the active layer are critical to device performance and that favorable morphology is more efficiently achieved in the thin film realm after thermal annealing.

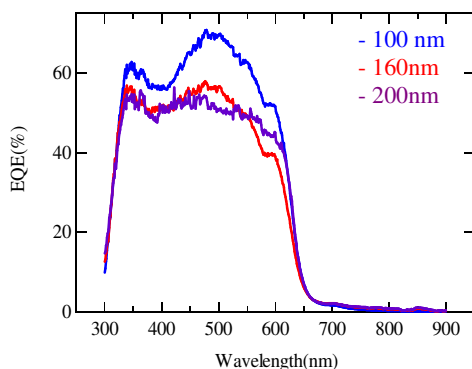


Figure 3. External quantum efficiency measurements for P3HT/PCBM heterojunction photovoltaic cells with different active layer thickness after solvent/thermal annealing. The device with a 100 nm-thick active layer shows maximum EQE of 67% at wavelength of ~500nm.

In these experiments, surface roughness was not found to be a critical factor in device performance. Atomic Force Microscopy yields surface roughnesses of 1.3 nm, 1.2 nm and 4.3 nm RMS for the 100, 160 and 200 nm active layers, respectively (Figure 4). The 100 and 160 nm films were comparably rough, while the 200 nm film was significantly rougher. Several groups in the past have noted enhanced device efficiency with greater surface roughness [5], but no such effect was observed in this work. If the effect is present, it is overshadowed by the efficiency drop that resulted from the altered shift in microstructure domains that resulted from the thermal annealing step.

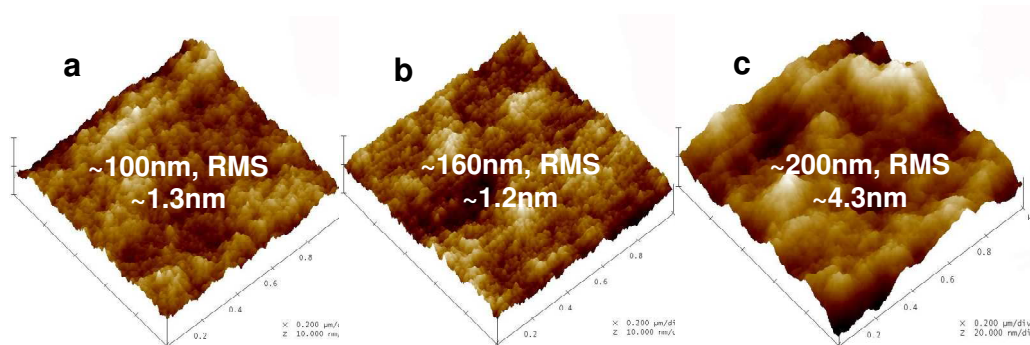


Figure 4. AFM surface morphology of P3HT/PCBM heterojunction photovoltaic cells after solvent/thermal annealing. The film thickness and surface roughness are marked on image (a), (b) and (c).

Understanding the mechanisms by which thermal and solvent annealing take place is paramount to continuing to improve device efficiencies. Ultimately, if thermal and solvent annealing techniques were optimized for thick-layer devices, the same polymer ordering (and corresponding charge carrier mobility and light absorption) and networking that exists in the thin-film realm could be achieved. Thus, current thickness limitations on performance in organic photovoltaic devices could be overcome and optimal thicker devices could be viably processed. Such a breakthrough would enable devices to absorb more light and generate more power, and represent a major step towards the development of photovoltaic devices.

CONCLUSIONS

We have shown that solvent vapor treatment improves the performance of 200 nm-thick layer devices more noticeably than thin-layer devices. Followed thermal annealing was found to be most beneficial in improving power efficiency of devices with active layer thicknesses in the range of 100 to 160 nm. We believe that this is due to a combined effect of polymer ordering and optimization of morphology/percolation in the blend film, which varies with film thickness and is sensitive to annealing treatments.

ACKNOWLEDGMENTS

The authors would like to thank Dr. George G. Malliaras and his research group at Cornell University for support of partial experiments. Funding for this project was provided by a grant from the National Aeronautics and Space Administration.

REFERENCES

1. Saricifti, N.S., Smilowitz, L. Heeger, A.J., Wudl, F. Science 258, 5987, 1474 (1992).

2. C. J. Brabec, A. Cravino, D. Meissner, N.S. Sariciftci, M.T. Rispens, L. Sanchez, J.C. Hummelen. *Thin Solid Films* 403-403, 368 (2002).
3. Brabec, C.J. *Solar Energy Materials and Solar Cells* 83, 273 (2004).
4. K. Kim, J. Liu, M. Namboothiry, D. Carroll. *Applied Phys. Letters* 90, 163511 (2007).
5. G. Li, Y. Yang *J. Appl. Phys.* 98, 043704 (2005).
6. T. Erb, U. Zhokhavets, H. Hope, G. Gobsch, M. Al-Ibrahim, O. Ambacher. *Ab Thin Solid Films* 511-512, 483 (2006).
7. Y. Kim, S. Cook, S.A. Choulis, J. Nelson, J.R. Durrant and D.D.C. Bradley. *Synthetic Metals* 152, 105 (2005).
8. H. Kim, W. So, S. Moon. *J. Korean Physical Society*, 48, 441 (2006).
9. T. Aernouts, P. Vanlacke, I. Haeldermans, J. D. Haen, P. Haremans, J. Poortmans, J. Mance. *Mater. Res. Soc. Symp. Proc. Vol. 1013* (2007).
10. M. Reyes-Reyes, K. Kim, D. Carroll. *Appl. Phys. Lett.* 87, 083506 (2005).
11. K. Yazawa, Y. Inoue, T. Yamamoto, N. Askawa, *Phys. Rev. B* 74, 094204 (2006).
12. M.R. Reyes, K. Kim, J. Dewald, R.L. Sandoval, A. Avadhanula, S. Curran, and D. L. Carroll. *Org. Lett.* 7, 5749 (2005).
13. P. Vanlaeke, A. Swinnen, I. Haeldermans, G. Vanhoyland, T. Aernouts, D. Cheyns, C. Deibel, J. D;Haen, P. Heremans, J. Poortmans and J.V. Manca *Solar Energy Materials & Solar Cells* 90, 2150 (2006).
14. K. Kim, J. Liu, M. Namboothiry, D. Carroll. *Appl. Phys. Lett.* 90, 163511 (2007).
15. Y. Kim, S. Cook, S.A. Choulis, J. Nelson, J.R. Durrant, D.D.C. Bradley. *Appl. Phys. Lett.* 86, 063502 (2005).
16. P. Vanlaeke, G. Vanhoyland, T. Aernouts, D. Cheyns, C. Deibel, J. Manca P. Heremans, J. Poortmans. *Thin Solid Films* 511-512, 358 (2006).
17. J. Huang, G. Li, Y. Yang. *Appl. Phys. Lett.* 87, 1121 05 (2005).
18. W. Ma, C. Yang, X. Gong, K. Lee, A. J. Heeger. *Adv. Func Mater.* 13, 85 (2003).
19. S. Miller*, G. Fanchini, Y. Lin, C. Li, C. Chen, W. Su and M. Chhowalla. *J Mater Chem*, 18, 306 (2008).
20. G. Li, Y. Yao, H. Yang, V. Shrotriya, G. Yang, Y. Yang *Adv. Funct. Mater.*, 17, 1636 (2007).
21. Yun Zhao, Zhiyuan Xie,a_ Yao Qu, Yanhou Geng, and Lixiang Wang. *Appl. Phys. Lett.* 90, 043504 (2007).